ACS NANO
Cite This: ACS Nano XXXX, XXX, XXX–XXX
www.acsnano.org

ARTICLE

Binary Phosphorene Redox Behavior in Oxidoreductase Enzymatic Systems

Carmen C. Mayorga-Martinez,[†] Zdeněk Sofer,[†] and Martin Pumera*[,†,‡,§]

[†]Center for Advanced Functional Nanorobots, Department of Inorganic Chemistry, Faculty of Chemical Technology, University of Chemistry and Technology in Prague, Technická 5, Prague 166 28, Czech Republic

[‡]Department of Medical Research, China Medical University Hospital, China Medical University, No. 91 Hsueh-Shih Road, Taichung 40402, Taiwan

[§]Future Energy and Innovation Laboratory, Central European Institute of Technology, Brno University of Technology, Purkyňova 656/123, Brno CZ-616 00, Czech Republic

ABSTRACT: **Phosphorene is a two-dimensional material that has many advantageous electronic, electrochemical, and optical properties. However, phosphorene possesses a relatively poor stability in ambient atmosphere. This disadvantage limits its application in several systems and particularly in electrochemical biosensors. Here we evaluate phosphorene as an electrochemical biosensing platform in two different mediator-based oxidoreductase enzymatic systems (glucose oxidase (GOx) and peroxidase from horseradish (HRP)), in which their detection is based on the reduction or oxidation of a mediator. In both cases, the used mediator is the same, ferrocene methanol (FcMeOH). Enhanced electrochemical activity is observed only in the reductive system (HRP-based biosensor) when compared to the oxidative counterpart (GOx-based biosensor). This phenomenon is attributed to the fact that in a reductive environment the phosphorene structure remains intact, while in an oxidative potential, the phosphorene is readily oxidized. In this way, the electroactivity of phosphorene as a sensing platform is strongly dependent on the type of mediator-based enzymatic system. These findings of binary nature of phosphorene are of high importance for construction of phosphorene-sensing platforms and in the development of enzyme logic systems.**

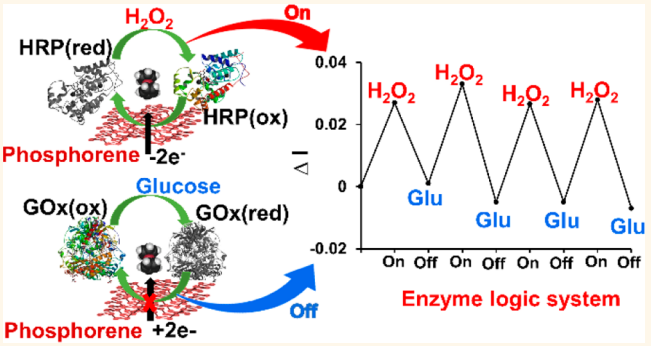

KEYWORDS: *black phosphorus, oxidoreductase enzymes, mediator-based enzymatic biosensor, second-generation biosensor*

The fascinating electrical, optical, and chemical properties of 2D materials have been explored for many applications in biomedical fields and energy generation and storage.[1−6] 2D materials play an important role in the development of advanced devices, such as sensors and biosensors.[2,3] In the area of bio/sensing applications, 2D materials doped[3−5] or decorated[7,8] with metal and nonmetal materials have been used to improve the device sensitivity, selectivity, and stability. However, the use of a simple design with pure 2D materials for bio/sensing purposes is in high demand.

Phosphorene is the most representative member of the two-dimensional pnictogen family,[1,2,9−16] and it is still widely studied since it was exfoliated for the first time in 2014.[9] This is due to its impressive electrical properties, which rank from semimetallic to semiconducting,[9] that can be applied in the development of many devices for gas sensing,[17] energy generation,[18] and storage.[19,20] However, phosphorene possesses a relatively poor stability in ambient atmosphere, because it is easily oxidized and it deteriorates in ambient atmosphere, which compromises its chemical structure and electronic properties.[21−23] For this reason, researchers have been exploring the mechanism of phosphorene instability and the strategies to protect phosphorene from ambient degradation in order for its structure to remain intact.[23] These strategies range from physical routes (passivation layers and capping using other 2D materials) to chemical routes (surface modification by organic compounds).[21,23] On the other hand, the low stability of phosphorene limited its application in many research areas and particularly in electrochemical research, where the high electrical conductivity and the electroactive properties of the material are imperative. This is the reason that the electrochemical biosensing applications of phosphorene found in the literature are limited,[24−28] which is unfortunate because phosphorene possesses so many advan-

Received: August 7, 2019
Accepted: October 4, 2019

DOI: 10.1021/acsnano.9b06230
ACS Nano XXXX, XXX, XXX–XXX

Scheme 1. Schematic representation of binary phosphorene behavior in oxidative or reductive second-generation enzymatic systems for the development of a highly sensitive H_2O_2 biosensor as well as an on/off enzymatic system.

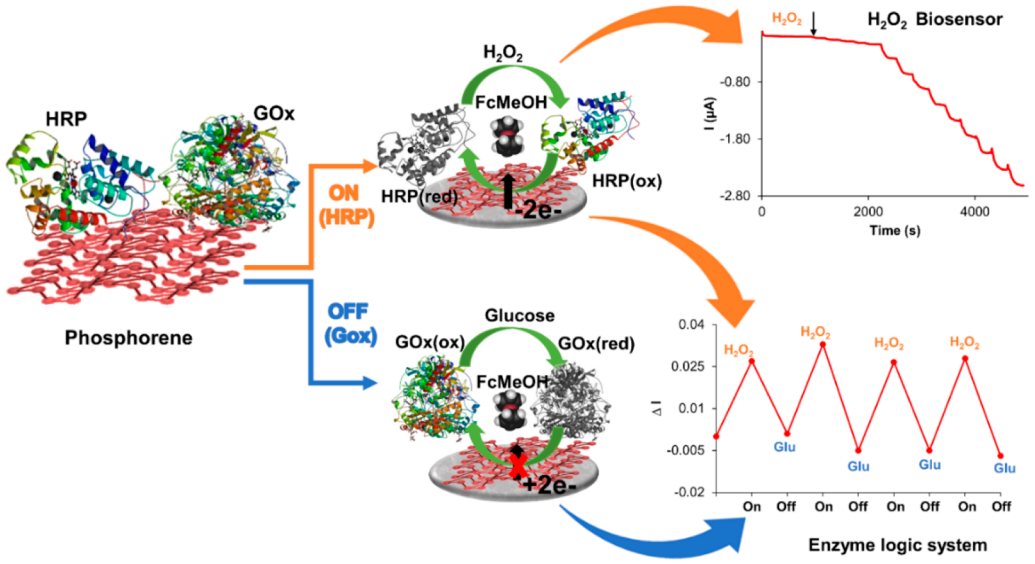

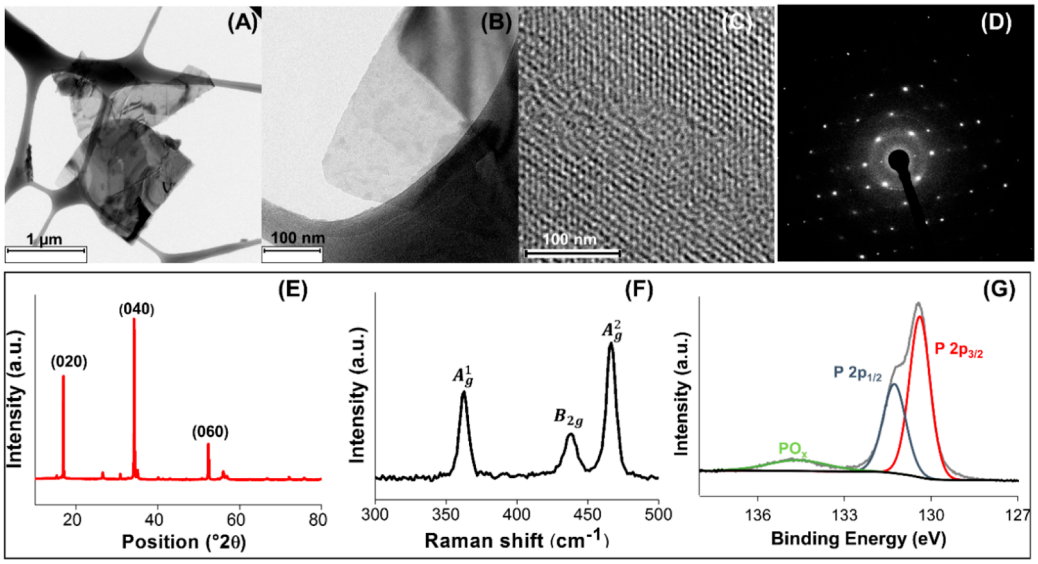

Figure 1. Morphological characterization: TEM at different magnifications (A and B), HR-TEM (C), and selected area diffraction (D) of BP nanosheets. Structural and chemical characterization: XRD (E), Raman (F), and HR-XPS (G) spectra of black phosphorus.

tages, such as high biocompatibility[29−32] as well as its unique photophysical, photochemical, and electrocatalytic properties that make this materials suitable for biomedical applications such as drug delivery,[33] phototherapy,[34−36] and biosensing.[24−28,30,37−39]

Here we implement phosphorene as a sensing platform in two mediator-based enzymatic biosensors. We took advantage of the high heterogeneous electron transfer properties of phosphorene to implement two different second-generation biosensors using glucose oxidase (GOx) and peroxidase from horseradish (HRP) to detect glucose and H_2O_2, respectively (see Scheme 1). Interestingly we observed that the phosphorene works efficiently as a platform exclusively for H_2O_2 detection biosensor with the signal coming from the electroreduction of the mediator (ferrocene methanol), whereas in the case of the biosensor for glucose detection, which is based on the electrooxidation of the mediator, the system did not show any enhancement. In a reductive environment, the phosphorene structure remains intact, while in an electro-oxidative environment its structure is compromised. Such a finding is used for the development of a highly sensitive H_2O_2 biosensor as well as on/off enzymatic systems.

RESULTS AND DISCUSSION

We used a high-quality few-layer phosphorene prepared by the vapor phase grow synthesis method,[40] and we exfoliated black phosphorus (BP) to phosphorene by sonication-assisted liquid exfoliation for 2 h.[1,18,41] The high quality of the materials is proved by systematic characterization studies using transmission electron microscopy (TEM), X-ray diffraction (XRD), Raman and X-ray photoelectron spectroscopy (XPS). The TEM images (Figure 1A and B) exhibit few-layer nanosheets with a lateral size of a few micrometers, whereas the high-resolution TEM (HR-TEM) and selective area electron

DOI: 10.1021/acsnano.9b06230
ACS Nano XXXX, XXX, XXX−XXX

diffraction (SAED) patterns, Figure 1C and D, show the orthorhombic crystalline structure, characteristic for high-quality phosphorene. The crystalline structure of BP was also evidencde by XRD studies (Figure 1E), in which the orthorhombic structure (*Cmca* space group; PDF card # 01-076-1957) with strong preferential orientation along the (0*k*0) direction and an extremely narrow diffraction pattern were observed, indicating its high crystallinity. On the other hand, the Raman spectrum (Figure 1F) shows the characteristic intensities of A_g^1 (361 cm^{-1}), B_{2g} (440 cm^{-1}), and A_g^2 (467 cm^{-1}). The low level of oxidation was demonstrated by XPS (Figure 1G), where the peak intensity of POx is negligible and the characteristic peak of P 2p that correspond to P−P bonding is observed.

After the high quality of phosphorene with a low level of oxidation was demonstrated, the heterogeneous electron transfer (HET) of black phosphorus in the presence of FcMeOH as a redox probe was studied. For this aim cyclic voltammograms were recorded in anodic (Figure 2A) and cathodic (Figure 2B) directions using a glassy carbon (GC) electrode modified with phosphorene as a working electrode. In both cases, the oxidative and reversible reductive peaks of FcMeOH were observed. Moreover, enhanced current intensities with regard to the glassy carbon electrode used as a control were observed. Besides, an inherent oxidative peak appears in both cyclic scans around 460 mV, which correspond to phosphorus oxidation from P^0 to P^{5+} with the production of H_3PO_4. The oxidative peaks observed in the initial anodic and cathodic sweeps disappear from subsequent scans (see Figure 2C and D), because the phosphorus oxidation is a chemically irreversible process.

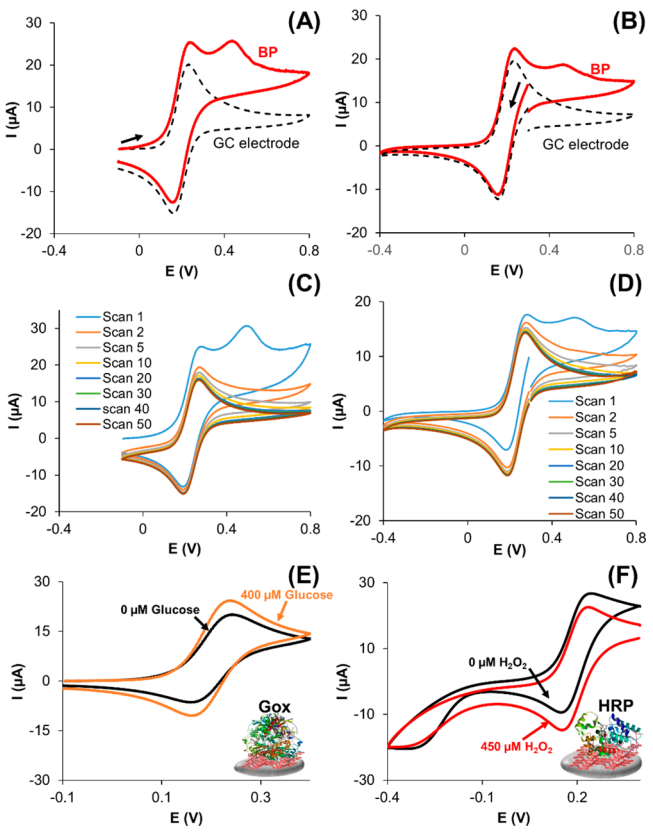

Figure 2. Cyclic voltammetry (CV) in the anodic (A) and cathodic (B) direction of phosphorene nanosheets and bare glassy carbon (GC) electrode as a control. Long-term cyclic stability in the anodic (C) and cathodic (D) direction of phosphorene. CV of the GC/BP/GOx biosensor in the absence and presence of 400 μM glucose (E) and CV of the GC/BP/HRP biosensor in the absence and presence of 450 μM H_2O_2 (F). Experimental conditions: PBS pH 7.2 and 2 mM ferrocene methanol, scan rate for the CV 50 mV/s.

Given that this mediation enhances the current of the redox probe (FcMeOH) on the phosphorene electrode, this allows to use it in a mediator-based enzymatic system. Two different enzymatic systems that operate using FcMeOH as mediator were implemented. The first system uses GOx for glucose detection, and the oxidation of the mediator was recorded (see Figure 2E). In the second system the reduction of the mediator was evaluated, and an HRP-based system for H_2O_2 detection was used (see Figure 2F).

In the first system, the flavin redox center of GOx was reduced in the presence of glucose, and eventually, the regeneration of oxidized GOx takes place using ferrocenium ion (Fc^+MeOH) as the mediator (eq 1). Finally, the interconversion of Fc^+MeOH to FcMeOH takes place on the phosphorene electrode surface, giving rise to an oxidation signal that relates to glucose concentration (eq 2); see Figure 2C.

$$\text{Glucose} + 2Fc^+\text{MeOH} + \frac{1}{2}O \xrightarrow{\text{GOx}} \text{gluconic acid} + 2\text{FcMeOH} + H_2O_2 + 2H^+ \quad (1)$$

$$2\text{FcMeOH} \xrightarrow[+200\text{ mV}]{} Fc^+\text{MeOH} + 2e^- \quad (2)$$

In the second system the HRP catalyzed the oxidation of FcMeOH to Fc^+MeOH in the presence of H_2O_2 (eq 3), and then Fc^+MeOH is rapidly electrochemically reduced at the electrode surface modified by phosphorene (eq 4); see Figure 2D.

$$2\text{FcMeOH} + H_2O_2 + 2H^+ \xrightarrow{\text{HRP}} 2Fc^+\text{MeOH} + 2H_2O \quad (3)$$

$$2Fc^+\text{MeOH} + 2e^- \xrightarrow[+100\text{ mV}]{} 2\text{FcMeOH} \quad (4)$$

To evaluate the efficiency of phosphorene as a sensing platform, chronoamperometry measurements are performed in both systems. In the case of the glucose detection system, +200 mV is chosen as a working potential. Interestingly, the presence of phosphorene as a platform in the biosensor does not enhance the recorded signal of FcMeOH oxidation (see orange line in Figure 3A) with regard to the signal recorded in the biosensor without phosphorene (black line in Figure 3A). Conversely, in the case of H_2O_2 detection using phosphorene as a platform, the signal recorded by applying +100 mV that corresponds to FcMeOH reduction is superior compared with the one obtained in the biosensor without phosphorene. Phosphorene at continuous oxidative potential conditions is degraded, and its electron transfer capability is compromised; for that reason in the glucose detection system implemented the signal is lower and unstable. Nevertheless, the reductive potential applied for FcMeOH reduction in the system based on HRP for H_2O_2 detection contributes to maintain and stabilize the BP structure. To confirm this assertion, two experiments are assayed: two GC electrodes are modified with

DOI: 10.1021/acsnano.9b06230
ACS Nano XXXX, XXX, XXX−XXX

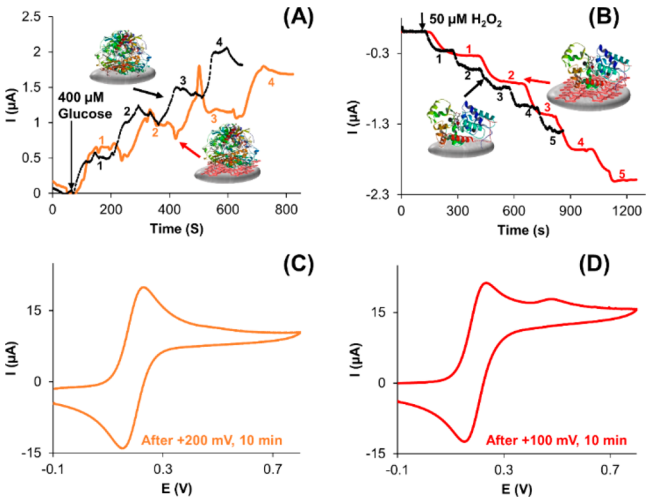

Figure 3. Chronoamperometry at +200 mV of the GC/BP/GOx biosensor and GC/GOx biosensor under successive additions of 400 μM glucose (A). Chronoamperometry at +100 mV of the GC/BP/HRP biosensor and GC/HRP biosensor under successive additions of 50 μM H_2O_2 (B). Cyclic voltammetry of GC electrodes modified with BP after applying +200 mV (C) and +100 mV (D) during 10 min. Experimental conditions: PBS pH 7.2 and 2 mM ferrocene methanol, scan rate for the CV 50 mV/s.

5 μg of phosphorene, each of them is immersed in two different electrochemical cells that contain a solution of phosphate-buffered saline (PBS) pH 7.2 and 2 mM ferrocene methanol, and +100 and +200 mV are applied, respectively, during 10 min. After each experiment the corresponding cyclic voltammetry (CV) scan is recorded (see Figure 3C and D). When +200 mV is applied, the recorded scan (Figure 3C) does not show the oxidation peak at ~460 mV, meaning that the BP is completely oxidized. However, in the CV scan measured after the phosphorene electrode is exposed at +100 mV, the oxidative peak around ~460 mV can be observed, which signifies the low oxidation of phosphorene, and this is the reason that the biosensing system for H_2O_2 is more efficient and stable, since the black phosphorus is not oxidized and preserves its structure under the reductive environment.

The logic enzymatic system allows the analysis of a complex sample using a digital biosensor by a biocomputing system. This biocomputing system mimics networked Boolean logic gates and can process chemical input signals in a digital arrangement (0/1), creating an off/on output signal that can produce an alert-type biosensing system. The biological marker inputs in a logic format are made in the biochemical domain and simplified the electronic computing systems for analyzing the biosensor response, increasing its fidelity and easy read-out responses, which allows obtaining digital biosensors for user-friendly point-of-care applications.[42,43]

As a simple application of our finding, we prepared a biosensor with both enzymes to demonstrate on/off behavior for a logic enzymatic system application. The chronoamperometric measurements were carried out at +100 mV (Figure 4A) and +200 mV (Figure 4C). H_2O_2 and glucose at a concentration of 50 μM are added in alternating way. When the chronoamperogram is recorded at +100 mV, a significant current change is observed after H_2O_2 addition, while in the presence of glucose the current did not change. If we compare the current change (ΔI) before and after each analyte is added, we obtain an "on/off" system (Figure 4B), where "on" is observed after H_2O_2 addition and "off" when glucose is added. A similar response is observed when +200 mV is applied

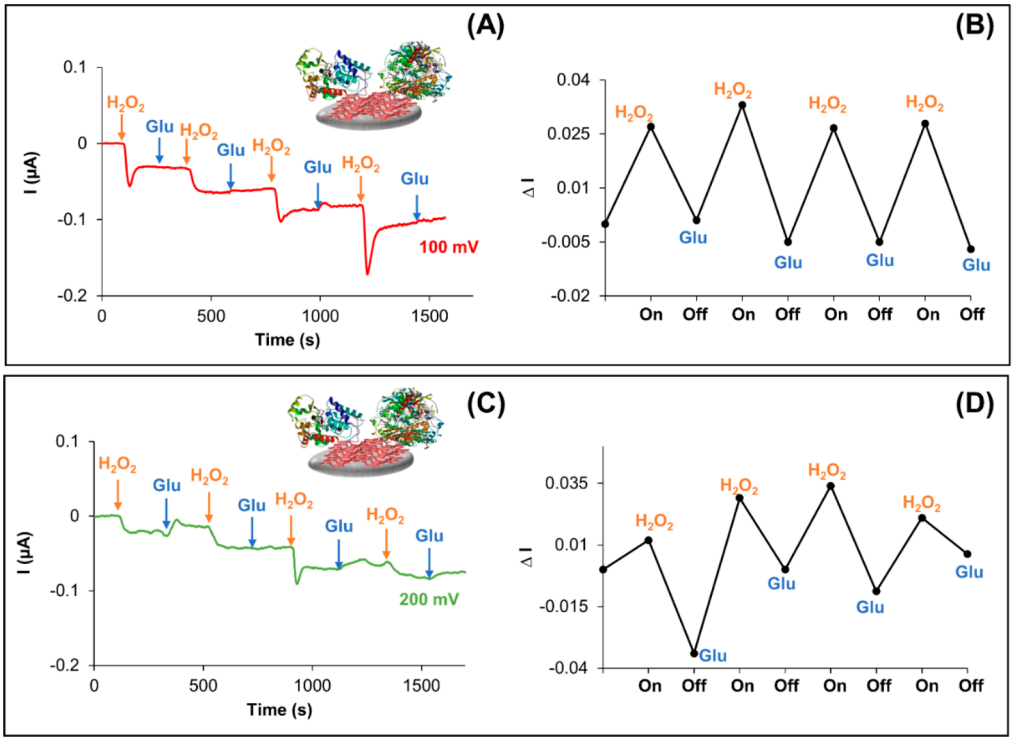

Figure 4. Chronoamperometry response recorded at +100 mV (A) and +200 mV (C) after alternating additions of H_2O_2 and glucose in PBS pH 7.2 and 2 mM ferrocene methanol: Comparison of current change before and after addition of H_2O_2 and glucose, when +100 mV (B) and +200 mV (B) are applied, respectively.

DOI: 10.1021/acsnano.9b06230
ACS Nano XXXX, XXX, XXX−XXX

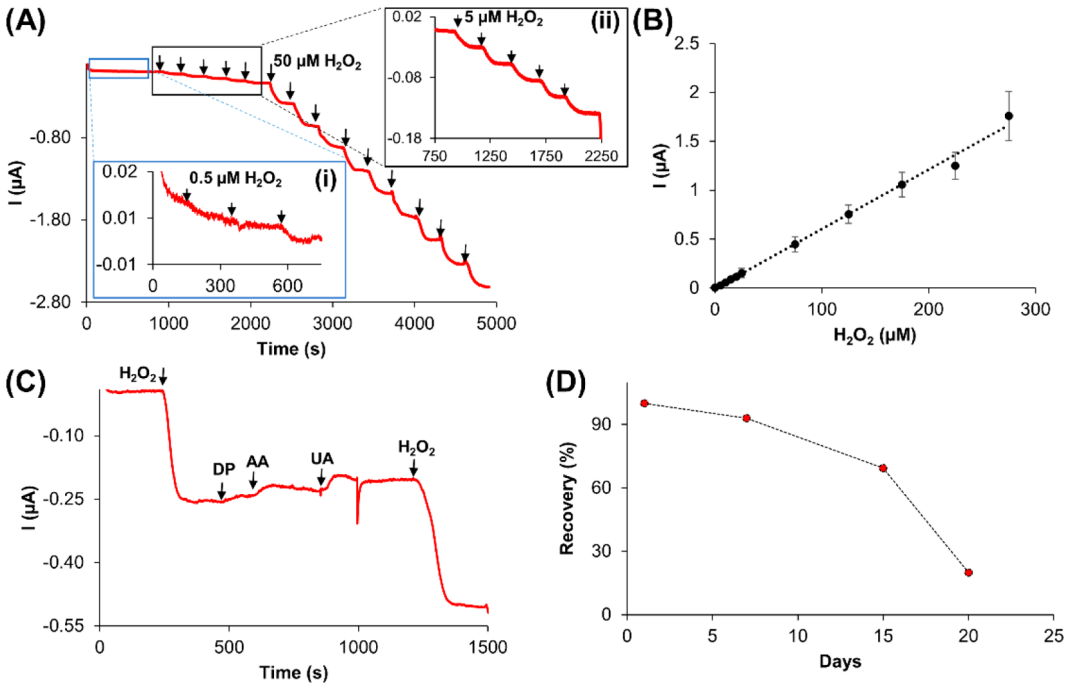

Figure 5. Chronoamperometry at +100 mV of the GC/BP/HRP biosensor under successive additions of different H_2O_2 concentrations (A). Calibration curve of the GC/BP/HRP biosensor (B). Selectivity study of the GC/BP/HRP biosensor in the presence of different interference species (C). Long-term stability of the GC/BP/HRP biosensor (D). Percentage recovery of the reductive current obtained in the presence of 50 μM H_2O_2 over 20 days.

(Figure 4C and D), but as expected, the signal was unstable, because the phosphorene was oxidizing. In the implemented logic enzymatic system, taking advantage of the low stability of phosphorene, under an oxidative environment the biosensor response is blocked, whereas in the reductive environment the biosensor can detect H_2O_2 efficiently in the presence of glucose also if the glucose oxidase is part of the biosensing system.

After we demonstrated the enhanced capability of phosphorene as a platform for H_2O_2 detection, we investigated also the analytical performance of the developed biosensor for H_2O_2 detection. Figure 5A shows the chronoamperogram of the GC/BP/HRP biosensor after the successive addition of different H_2O_2 concentrations. In the first 750 s, 0.5 μM H_2O_2 was added three times (see inset (i) in Figure 5A). A small current change can be observed after the first and the second additions, and a significant change is observed after the third addition, which corresponds to cumulative concentrations of 1.5 μM H_2O_2. This demonstrates the high sensitivity of the implemented phosphorene-based biosensor system. After the addition of a higher concentration (5 μM H_2O_2), the typical current steps are observed (see inset (ii) in Figure 5A). Finally, when the H_2O_2 concentration is increased to 50 μM, the current response is more evident for each addition and the biosensor response is very fast (~200 s). Interestingly, after eight continuous additions the system is not saturated, which is possibly due to BP being continuously reduced under this reductive environment.

The calibration curve represented in Figure 5B is prepared from the chronoamperogram (Figure 5A) that was repeated for three different biosensors (RSD ~15%). A wide concentration range for H_2O_2 detection was observed with a good linearity (r = 0.9970) and low limit of detection of 0.14 μM (Table1). Moreover, this system shows a low apparent Michaelis–Menten constant (k_M^{app}) of 164 μM, which demonstrated the high affinity of this enzymatic system to H_2O_2. Finally, this system shows high selectivity, which is due to the low working potential of the system (+100 mV), and the main interferences are biomolecules that are oxidized at positive potentials. Figure 5C shows a chronoamperogram of the successive additions of 50 μM H_2O_2, 100 μM dopamine (DP), 100 μM ascorbic acid (AA), 100 μM uric acid (UA), and 50 μM H_2O_2 into stirred PBS pH 7.2 with 2 mM ferrocene methanol. All the interference species studies show a negligible signal, demonstrating the high selectivity of the biosensor toward the analyte.

Table 1. Analytical Performance Comparison of HRP and 2D Materials-Based Biosensors for H_2O_2 Biosensing

2D material	method	lineal ranges [μM]	LOD [μM]	ref
MoS_2-graphene	chronoamperometry	0.2–1103	0.049	53
MoS_2	DPV	1–95	0.26	54
1T-WS_2/TiO_2	chronoamperometry	0.5–30 50–300	8.5	52
phosphorene	chronoamperometry	5–275	0.14	this work

The enzyme immobilization in the enzyme-based biosensor technology has been an important research topic for the last 50 years. In this process the enzyme or multiple enzyme systems are confined in the surface of a transducer as an insoluble film that retains intact their catalytic activity. Several methods were reported for this aim, such as that reported by Okahata *et al.* in 1988, where they created a glucose oxidase–lipid complex formed as stable Langmuir–Blodgett (LB) films[44] or that reported by Onda *et al.* in 1996 for the production of molecular films of proteins/polyion layers, assembled in alternative adsorption through electrostatic interactions.[45,46]

DOI: 10.1021/acsnano.9b06230
ACS Nano XXXX, XXX, XXX–XXX

The last method was used to assemble two enzymes together (glucose oxidase and peroxidase[45] or glucoamylase and glucose oxidase[46]). Later the enzyme immobilization by covalent attachment *via* glutaraldehyde represented one of the simplest and gentlest methods reported and was used widely in enzyme-based biosensor technology.[47−52] This cross-linking agent can react with the amine groups of the enzyme in buffer solution under conditions close to physiological pH, ionic strength, and temperature.[47]

In this work, we immobilized the enzymes *via* a cross-linking method. The long-term stability of the GC/BP/HRP biosensor was evaluated and is represented in Figure 5D. The biosensor displayed good stability, as it retained 93% of its initial current response after 7 days, but after 15 days the retention rate dropped to 69%. This was evidence that the enzyme structure was not denatured after immobilization by cross-linking and retained its activity. On the other hand, the chronoamperometry measurements for H_2O_2 detection were continuously done for 100 min (Figure 5A), which is another proof that the catalytic activity of the enzyme was not compromised during the immobilization process.

H_2O_2 is an oxidative stress marker and a main reactive oxygen species (ROS) reported in living cells. For that reason it is very important to develop highly sensitive, specific, and cost-efficient devices for H_2O_2 testing. In this way, the developed biosensor in this work exhibited good analytical performance when compared with preceding reports of hydrogen peroxide sensing. In Table 1 we compared our biosensor with other electrochemical biosensors based on 2D materials and HRP. The explanation of the high performance of this phosphorene-based H_2O_2 biosensor is probably that the BP is continuously reduced under this reductive environment.

On the other hand, H_2O_2 detection by the HRP-based biosensor has been used for label-based electrochemical detections of proteins, toxins, or DNA where the HRP acts as a label.[55−57] In this way we are convinced that our system can be implemented for the detection of proteins, toxins, and DNA detection as well, in a similar manner to the phosphorene analogue antimonene, which was reported recently for highly sensitive miRNA detection.[58]

CONCLUSIONS

We evaluated phosphorene as a transducer platform for two mediator-based enzymatic systems. The first one uses the enzyme glucose oxidase, and the glucose was indirectly detected by mediator oxidation. The second system uses HRP, and the H_2O_2 detection was based on the reduction of the mediator. In both systems, we use the same mediator, ferrocene methanol, but the phosphorene showed dramatically different behavior in the oxidative and reductive enzymatic setup. We have demonstrated that phosphorene works efficiently as a sensing platform in the reductive system. In that way, we developed an on/off system based on a bioenzymatic biosensor composed for both enzymes (GOx and HRP) as well as a sensitive and selective H_2O_2 biosensor. Such findings of a binary nature of black phosphorene will have a profound influence on the construction of phosphorene-based biosensors and enzyme logic systems.

METHODS

Reagents and Apparatus. For the synthesis of black phosphorus, red phosphorus (99.999%) and tin (99.999%) were purchased from Sigma-Aldrich; iodine (99.9%), carbon disulfide (99.99%), and chloroform (99.9%) were obtained from Penta, Czech Republic. The biosensor was prepared using peroxidase from horseradish (lyophilized powder, ≥250 unit/mg, Sigma-Aldrich, Czech Republic) and glutaraldehyde solution (grade I, 70% in H_2O, Sigma-Aldrich, Czech Republic). The electrochemical measurements were performed in 0.1 M phosphate buffer pH 7.2 with 0.1 M KCl and 2 mM ferrocene methanol that was prepared using potassium dihydrogen phosphate, potassium monohydrogen phosphate dehydrate, potassium chloride, and ferrocene methanol, which were purchased from Sigma-Aldrich, Czech Republic.

For the electrochemical measurements, an Autolab PGSTAT204/FRA32 M (Eco Chemie, Utrecht, from The Netherlands) was used. HR-TEM was obtained using a transmission electron microscope (JEOL JEM 2200FS). The microscope was operated at 200 kV (autoemission Schottky gun, point resolution 0.19 nm) with an in-column energy Ω-filter for EELS/EFTEM analyses. XPS measurements were made with a Phoibos 100 spectrometer and a monochromatic Mg X-ray radiation source (SPECS, Germany). Raman spectra were performed with a confocal micro-Raman LabRam HR instrument (Horiba Scientific) in backscattering geometry, and a CCD detector was used. An Olympus optical microscope was used with a 514.5 nm Ar laser and a 100× objective attached. The calibration was achieved using an internal silicon reference at 520 cm^{-1} with a peak position resolution of less than 1 cm^{-1}.

Black Phosphorus Synthesis. The black phosphorus was synthesized by a vapor-phase growth method. First, SnI4 was prepared by refluxing iodine and tin in chloroform, and SnI_4 was obtained by recrystallization from chloroform. Later, a mixture of SnI_4 (20 mg), red phosphorus (500 mg), and Sn (40 g) was placed inside a quartz ampule. The ampule was sealed by an oxygen/hydrogen torch and heated at 400 °C for 3 h in a muffle furnace. The temperature was increased to 600 °C and maintained for 24 h. Afterward, the ampule was cooled until it reached room temperature. The resulting material was washed with CS_2.

Biosensor Preparation. The biosensor was prepared by drop-casting 5 μg of BP (diluted in *N*,*N*-dimethylformamide (DMF)), 0.1 μg of HRP, or GOx and 5 μL of glutaraldehyde (1%) onto a GC electrode. After the first and second steps, the materials were dried under 30 °C for 1 h, and, after the drop-casted glutaraldehyde, the electrode was dried at 40 °C for 1 h. To overcome the easy oxidation of the black phosphorus, BP is sonicated in DMF and fresh solutions were always used for preparing the biosensors.

AUTHOR INFORMATION

Corresponding Author

*E-mail: Pumera.group@gmail.com, martin.pumera@ceitec.vutbr.cz.

ORCID

Carmen C. Mayorga-Martinez: 0000-0003-3687-0035

Zdeněk Sofer: 0000-0002-1391-4448

Martin Pumera: 0000-0001-5846-2951

Notes

The authors declare no competing financial interest.

ACKNOWLEDGMENTS

M.P. acknowledges the financial support of the Grant Agency of the Czech Republic (EXPRO: 19-26896X).

REFERENCES

(1) Tan, C.; Cao, X.; Wu, X.-J.; He, Q.; Yang, J.; Zhang, X.; Chen, J.; Zhao, W.; Han, S.; Nam, G.-H.; Sindoro, M.; Zhan, H. Recent Advances in Ultrathin Two-Dimensional Nanomaterials. *Chem. Rev.* **2017**, *117*, 6225−6331.

(2) Chia, X.; Pumera, M. Characteristics and Performance of Two-Dimensional Materials for Electrocatalysis. *Nat. Catal.* **2018**, *1*, 909−921.

DOI: 10.1021/acsnano.9b06230
ACS Nano XXXX, XXX, XXX−XXX

(3) Khan, A. H.; Ghosh, S.; Pradhan, B.; Dalui, A.; Shrestha, L. K.; Acharya, S.; Ariga, K. Two-Dimensional (2D) Nanomaterials Towards Electrochemical Nanoarchitectonics in Energy-Related Applications. *Bull. Chem. Soc. Jpn.* **2017**, *90*, 627−648.
(4) Tan, S. M.; Pumera, M. Two-Dimensional Materials on the Rocks: Positive and Negative Role of Dopants and Impurities in Electrochemistry. *ACS Nano* **2019**, *13*, 2681−2728.
(5) Rao, C. N. R.; Pramoda, K. Borocarbonitrides, BxCyNz, 2D Nanocomposites with Novel Properties. *Bull. Chem. Soc. Jpn.* **2019**, *92*, 441−468.
(6) Akinwande, D.; Petrone, N.; Hone, J. Two-Dimensional Flexible Nanoelectronics. *Nat. Commun.* **2014**, *5*, 5678.
(7) Govindasamy, M.; Mani, V.; Chen, S. M.; Karthik, R.; Manibalan, K.; Umamaheswari, R. MoS_2 Flowers Grown on Graphene/Carbon Nanotubes: a Versatile Substrate for Electrochemical Determination of Hydrogen Peroxide. *Int. J. Electrochem. Sci.* **2016**, *11*, 2954−2961.
(8) Chao, J.; Zou, M.; Zhang, C.; Sun, H.; Pan, D.; Pei, H.; Su, S.; Yuwen, L.; Fan, C.; Wang, L. A MoS_2-Based System for Efficient Immobilization of Hemoglobin and Biosensing Applications. *Nanotechnology* **2015**, *26*, 274005.
(9) Gusmão, R.; Sofer, Z.; Pumera, M. Black Phosphorus Rediscovered: From Bulk Material to Monolayers. *Angew. Chem., Int. Ed.* **2017**, *56*, 8052−8072.
(10) Bagheri, S.; Mansouri, N.; Aghaie, E. Phosphorene: A New Competitor for Graphene. *Int. J. Hydrogen Energy* **2016**, *41*, 4085−4095.
(11) Lee, J.; Tian, W.-C.; Wang, W.-L.; Yao, D.-X. Two-Dimensional Pnictogen Honeycomb Lattice: Structure, On-Site Spin-Orbit Coupling and Spin Polarization. *Sci. Rep.* **2015**, *5*, 11512.
(12) Sorkin, V.; Cai, Y.; Ong, Z.; Zhang, G.; Zhang, Y. W. Recent Advances in the Study of Phosphorene and its Nanostructures. *Crit. Rev. Solid State Mater. Sci.* **2017**, *42*, 1−82.
(13) Kuriakose, S.; Ahmed, T.; Balendhran, S.; Bansal, V.; Sriram, S.; Bhaskaran, M.; Walia, S. Black Phosphorus: Ambient Degradation and Strategies for Protection. *2D Mater.* **2018**, *5*, 032001.
(14) Yang, A.; Wang, D.; Wang, X.; Zhang, D.; Koratkar, N.; Rong, M. Recent Advances in Phosphorene as a Sensing Material. *Nano Today* **2018**, *20*, 13−32.
(15) Khandelwal, A.; Mani, K.; Karigerasi, M. H.; Lahiri, I. Phosphorene − The Two-Dimensional Black Phosphorous: Properties, Synthesis and Applications. *Mater. Sci. Eng., B* **2017**, *221*, 17−34.
(16) Yi, Y.; Yu, X.-F.; Zhou, W.; Wang, J.; Chu, P. K. Two-Dimensional Black Phosphorus: Synthesis, Modification, Properties, and Applications. *Mater. Sci. Eng., R* **2017**, *120*, 1−33.
(17) Mayorga-Martinez, C. C.; Sofer, Z.; Pumera, M. Layered Black Phosphorus as a Selective Vapor Sensor. *Angew. Chem., Int. Ed.* **2015**, *54*, 1−5.
(18) Ren, X.; Zhou, J.; Xiang, Q.; Liu, Y.; Huang, Z.; Li, Z.; Ge, Y.; Dhanabalan, S. C.; Ponraj, J. S.; Wang, S.; Zhong, J.; Zhang, H. Few-Layer Black Phosphorus Nanosheets as Electrocatalysts for Highly Efficient Oxygen Evolution Reaction. *Adv. Energy Mater.* **2017**, *7*, 1700396.
(19) Chen, L.; Zhou, G.; Liu, Z.; Ma, X.; Chen, J.; Zhang, Z.; Ma, X.; Li, F.; Cheng, H.-M.; Ren, K. Scalable Clean Exfoliation of High-Quality Few-Layer Black Phosphorus for a Flexible Lithium Ion Battery. *Adv. Mater.* **2016**, *28*, 510−517.
(20) Sajedi-Moghaddam, A.; Mayorga-Martinez, C. C.; Sofer, Z.; Bouša, D.; Saievar-Iranizad, E.; Pumera, M. Black Phosphorus Nanoflakes/Polyaniline Hybrid Material for High-Performance Pseudocapacitors. *J. Phys. Chem. C* **2017**, *121*, 20532−20538.
(21) Gusmão, R.; Sofer, Z.; Pumera, M. Functional Protection of Exfoliated Black Phosphorus by Noncovalent Modification with Anthraquinone. *ACS Nano* **2018**, *12*, 5666−5673.
(22) Plutnar, J.; Sofer, Z.; Pumera, M. Products of Degradation of Black Phosphorus in Protic Solvents. *ACS Nano* **2018**, *12*, 8390−8396.
(23) Kuriakose, S.; Ahmed, T.; Balendhran, S.; Bansal, V.; Sriram, S.; Bhaskaran, M.; Walia, S. Black Phosphorus: Ambient Degradation and Strategies for Protection. *2D Mater.* **2018**, *5*, 032001.
(24) Kumar, V.; Brent, J. R.; Shorie, M.; Kaur, H.; Chadha, G.; Thomas, A. G.; Lewis, E. A.; Rooney, A. P.; Lan, N.; Xiang, L. Z. Nanostructured Aptamer-Functionalized Black Phosphorus Sensing Platform for Label-Free Detection of Myoglobin, a Cardiovascular Disease Biomarker. *ACS Appl. Mater. Interfaces* **2016**, *8*, 22860−22868.
(25) Mayorga-Martinez, C. C.; Gusmão, R.; Sofer, Z.; Pumera, M. Pnictogen-Based Enzymatic Phenol Biosensors: Phosphorene, Arsenene, Antimonene, and Bismuthene. *Angew. Chem., Int. Ed.* **2019**, *58*, 134−138.
(26) Yan, S.; Wang, B.; Wang, Z.; Hu, D.; Xu, X.; Wang, J.; Shi, Y. Supercritical Carbon Dioxide-Assisted Rapid Synthesis of Few-Layer Black Phosphorus for Hydrogen Peroxide Sensing. *Biosens. Bioelectron.* **2016**, *80*, 34−38.
(27) Chen, Y.; Ren, R.; Pu, H.; Chang, J.; Mao, S.; Chen, J. Field-Effect Transistor Biosensors with Two-Dimensional Black Phosphorus Nanosheets. *Biosens. Bioelectron.* **2017**, *89*, 505−510.
(28) Mayorga-Martinez, C. C.; Latiff, N. M.; Eng, A. Y. S.; Sofer, Z.; Pumera, M. Black Phosphorus Nanoparticle Labels for Immunoassays *via* Hydrogen Evolution Reaction Mediation. *Anal. Chem.* **2016**, *88*, 10074−10079.
(29) Qiu, M.; Ren, W. X.; Jeong, T.; Won, M.; Park, G. Y.; Sang, D. K.; Liu, L.-P.; Zhang, H.; Kim, J. S. Omnipotent Phosphorene: A Next-Generation, Two-Dimensional Nanoplatform for Multidisciplinary Biomedical Applications. *Chem. Soc. Rev.* **2018**, *47*, 5588−5601.
(30) Qiu, M.; Singh, A.; Wang, D.; Qu, J.; Swihart, M.; Zhang, H.; Prasad, P. N. Biocompatible and Biodegradable Inorganic Nanostructures for Nanomedicine: Silicon and Black Phosphorus. *Nano Today* **2019**, *25*, 135−155.
(31) Latiff, N. M.; Mayorga-Martinez, C. C.; Sofer, Z.; Fisher, A. C.; Pumera, M. Cytotoxicity of Phosphorus Allotropes (Black, Violet, Red). *Appl. Mater. Today* **2018**, *13*, 310−319.
(32) Latiff, N. M.; Teo, W. Z.; Sofer, Z.; Fisher, A. C.; Pumera, M. The Cytotoxicity of Layered Black Phosphorus. *Chem. - Eur. J.* **2015**, *21*, 13991−13995.
(33) Chen, W.; Ouyang, J.; Liu, H.; Chen, M.; Zeng, K.; Sheng, J.; Liu, Z.; Han, Y.; Wang, L.; Li, J.; Deng, L.; Liu, Y.-N.; Guo, S. Black Phosphorus Nanosheet-Based Drug Delivery System for Synergistic Photodynamic/Photothermal/Chemotherapy of Cancer. *Adv. Mater.* **2017**, *29*, 1603864.
(34) Wang, X.; Shao, J.; Raouf, M. A. E.; Xie, H.; Huang, H.; Wang, H.; Chu, P. K.; Yu, X.-F.; Yang, Y.; AbdEl-Aal, A. M.; Mekkawy, N. H. M.; Miron, R. J.; Zhang, Y. Near-Infrared Light-Triggered Drug Delivery System Based on Black Phosphorus for *In Vivo* Bone Regeneration. *Biomaterials* **2018**, *179*, 164−174.
(35) Qiu, M.; Wang, D.; Liang, W.; Liu, L.; Zhang, Y.; Chen, X.; Sang, D. K.; Xing, C.; Li, Z.; Dong, B.; Xing, F.; Fan, D.; Bao, S.; Zhang, H.; Cao, Y. Novel Concept of the Smart NIR-Light−Controlled Drug Release of Black Phosphorus Nanostructure for Cancer Therapy. *Proc. Natl. Acad. Sci. U. S. A.* **2018**, *3*, 501−506.
(36) Choi, J. R.; Yong, K. W.; Choi, J. Y.; Nilghaz, A.; Lin, Y.; Xu, J.; Lu, X. Black Phosphorus and its Biomedical Applications. *Theranostics* **2018**, *8*, 1005−1026.
(37) Ying, T. Y.; Sofer, Z.; Mayorga Martinez, C. C.; Pumera, M. Black Phosphorus Nanoparticles as a Novel Fluorescent Sensing Platform for Nucleic Acid Detection. *Mater. Chem. Front.* **2017**, *1*, 1130−1136.
(38) Peng, J.; Lai, Y. Q.; Chen, Y. Y.; Xu, J.; Sun, L. P.; Weng, J. Sensitive Detection of Carcinoembryonic Antigen Using Stability-Limited Few-Layer Black Phosphorus as an Electron Donor and a Reservoir. *Small* **2017**, *13*, 1−11.
(39) Zhou, J.; Li, Z.; Ying, M.; Liu, M.; Wang, X.; Wang, X.; Cao, L.; Zhang, H.; Xu, G. Black Phosphorus Nanosheets for Rapid MicroRNA Detection. *Nanoscale* **2018**, *10*, 5060−5064.
(40) Mayorga-Martinez, C. C.; Sofer, Z.; Sedmidubský, D.; Luxa, J.; Kherzi, B.; Pumera, M. Metallic Impurities in Black Phosphorus

DOI: 10.1021/acsnano.9b06230
ACS Nano XXXX, XXX, XXX−XXX

Nanoflakes Prepared by Different Synthetic Routes. *Nanoscale* **2018**, *10*, 1540−1546.
(41) Lin, S.; Chui, Y.; Li, Y.; Lau, S. P. Liquid-Phase Exfoliation of Black Phosphorus and Its Applications. *FlatChem.* **2017**, *2*, 15−37.
(42) Halámek, J.; Zhou, J.; Halámková, L.; Bocharova, V.; Privman, V.; Wang, J.; Katz, E. Biomolecular Filters for Improved Separation of Output Signals in Enzyme Logic Systems Applied to Biomedical Analysis. *Anal. Chem.* **2011**, *83*, 8383−8386.
(43) Windmiller, J. R.; Santhosh, P.; Katz, E.; Wang, J. Bioelectronic System for the Control and Readout of Enzyme Logic Gates. *Sens. Actuators, B* **2011**, *155*, 206−213.
(44) Okahata, Y.; Tsuruta, T.; Ijiro, K.; Ariga, K. Langmuir-Blodgett Films of an Enzyme-Lipid Complex for Sensor Membranes. *Langmuir* **1988**, *4*, 1373−1375.
(45) Onda, M.; Lvov, Y.; Ariga, K.; Kunitake, T. Sequential Actions of Glucose Oxidase and Peroxidase in Molecular Films Assembled by Layer-by-Layer Alternate Adsorption. *Biotechnol. Bioeng.* **1996**, *51*, 163−167.
(46) Onda, M.; Lvov, Y.; Ariga, K.; Kunitake, T. Sequential Reaction and Product Separation on Molecular Films of Glucoamylase and Glucose Oxidase Assembled on an Ultrafilter. *J. Ferment. Bioeng.* **1996**, *82*, 502−506.
(47) Migneault, I.; Dartiguenave, C.; Bertrand, M. J.; Waldron, K. C. Glutaraldehyde: Behavior in Aqueous Solution, Reaction with Proteins, and Application to Enzyme Crosslinking. *BioTechniques* **2004**, *37*, 790−802.
(48) Barbosa, O.; Ortiz, C.; Berenguer-Murcia, A.; Torres, R.; Rodrigues, R. C.; Fernandez-Lafuente, R. Glutaraldehyde in Bio-Catalysts Design: a Useful Crosslinker and a Versatile Tool in Enzyme Immobilization. *RSC Adv.* **2014**, *4*, 1583−1600.
(49) López-Gallego, F.; Betancor, L.; Mateo, C.; Hidalgo, A.; Alonso-Morales, N.; Dellamora-Ortiz, G.; Guisán, J. M.; Fernández-Lafuente, R. Enzyme Stabilization by Glutaraldehyde Crosslinking of Adsorbed Proteins on Aminated Supports. *J. Biotechnol.* **2005**, *119*, 70−75.
(50) Rohaizad, N.; Mayorga-Martinez, C. C.; Sofer, Z.; Pumera, M. 1T-Phase Transition Metal Dichalcogenides (MoS_2, $MoSe_2$, WS_2, and WSe_2) with Fast Heterogeneous Electron Transfer: Application on Second-Generation Enzyme-Based Biosensor. *ACS Appl. Mater. Interfaces* **2017**, *9*, 40697−40706.
(51) Toh, R. J.; Mayorga-Martinez, C. C.; Sofer, Z.; Pumera, M. 1T-Phase WS_2 Protein-Based Biosensor. *Adv. Funct. Mater.* **2017**, *27*, 1604923.
(52) Rahmanian, E.; Mayorga-Martinez, C. C.; Malekfar, R.; Luxa, J.; Sofer, Z.; Pumera, M. 1T-Phase Tungsten Chalcogenides (WS_2, WSe_2, WTe_2) Decorated with TiO_2 Nanoplatelets with Enhanced Electron Transfer Activity for Biosensing Applications. *ACS Appl. Nano Mater.* **2018**, *112*, 7006−7015.
(53) Song, H.; Ni, Y.; Kokot, S. Investigations of an Electrochemical Platform Based on the Layered MoS_2−Graphene and Horseradish Peroxidase Nanocomposite for Direct Electrochemistry and Electrocatalysis. *Biosens. Bioelectron.* **2014**, *56*, 137−143.
(54) Wang, G.-X.; Bao, W.-J.; Wang, J.; Lu, Q.-Q.; Xia, X.-H. Immobilization and Catalytic Activity of Horseradish Peroxidase on Molybdenum Disulfide Nanosheets Modified Electrode. *Electrochem. Commun.* **2013**, *35*, 146−148.
(55) Wang, Z.; Yang, Y.; Leng, K.; Li, J.; Zheng, F.; Shen, G.; Yu, R. A. Sequence-Selective Electrochemical DNA Biosensor Based on HRP-Labeled Probe for Colorectal Cancer DNA Detection. *Anal. Lett.* **2008**, *41*, 24−35.
(56) Zhao, Y.; Zheng, Y.; Kong, R.; Xia, L.; Qu, F. Ultrasensitive Electrochemical Immunosensor Based on Horseradish Peroxidase (HRP)-Loaded Silica-Poly(Acrylic Acid) Brushes for Protein Biomarker Detection. *Biosens. Bioelectron.* **2016**, *75*, 383−388.
(57) Medina-Sánchez, M.; Mayorga-Martinez, C. C.; Watanabe, T.; Ivandini, T. A.; Honda, Y.; Pino, F.; Nakata, K.; Fujishima, A.; Einaga, Y.; Merkoçi, A. Microfluidic Platform for Environmental Contaminants Sensing and Degradation Based on Boron Doped Diamond Electrode. *Biosens. Bioelectron.* **2016**, *75*, 365−374.
(58) Xue, T.; Liang, W.; Li, Y.; Sun, Y.; Xiang, Y.; Zhang, Y.; Dai, Z.; Duo, Y.; Wu, L.; Qi, K.; Shivananju, B. N.; Zhang, L.; Cui, X.; Zhang, H.; Bao, Q. Ultrasensitive Detection of miRNA with an Antimonene-Based Surface Plasmon Resonance Sensor. *Nat. Commun.* **2019**, *10*, 28.

DOI: 10.1021/acsnano.9b06230
ACS Nano XXXX, XXX, XXX−XXX